available at www.sciencedirect.com

ScienceDirect

journal homepage: www.elsevier.com/locate/chnjc

Article

Photocatalytic degradation of bisphenol A using Ti-substituted hydroxyapatite

Qian Li [a], Xiang Feng [a], Xiao Zhang [a], Han Song [a], Jianwei Zhang [a], Jing Shang [a,*], Weiling Sun [a], Tong Zhu [a], Masato Wakamura [b], Mineharu Tsukada [b], Yingliang Lu [c]

[a] *College of Environmental Sciences and Engineering, Peking University, Beijing 100871, China*
[b] *Environment and Energy Research Center, Fujitsu Laboratories Limited, Atsugi, Japan*
[c] *Fujitsu Research and Development Center Company Limited, Beijing 100025, China*

ARTICLE INFO

Article history:
Received 22 July 2013
Accepted 11 September 2013
Published 20 January 2014

Keywords:
Titanium-substituted hydroxyapatite
Photocatalysis
Bisphenol A
Adsorption
Titanium dioxide

ABSTRACT

Ti-substituted hydroxyapatite (TiHAP) is a new photocatalyst with high adsorption capacity and photocatalytic activity. The morphology and structure of TiHAP were characterized using transmission electron microscopy, X-ray diffraction, ultraviolet-visible spectrophotometry, and the zeta potential. The adsorption and photocatalytic degradation of bisphenol A (BPA, an environmental endocrine disrupting chemical) over TiHAP and P25 TiO_2 photocatalysts were studied using liquid chromatography-mass spectrometry. The influences of fulvic acid and Fe^{3+} ions on the BPA degradation rate were analyzed. The adsorption of BPA on TiHAP and TiO_2 obeyed the Langmuir adsorption equation. TiHAP exhibited much higher adsorption capacity and photocatalytic degradation activity of BPA than TiO_2. Fulvic acid and Fe^{3+} showed different effects on the photocatalytic activity of TiHAP and TiO_2 films. These were explained by band structure theory, the electron transfer path, and optical absorption capacity. The results are useful for the application of TiHAP in the photocatalytic degradation of environmental endocrine disrupting chemicals.

1. Introduction

Bisphenol A (BPA) is a common industrial raw material widely used in the manufacturing of epoxy resin, polycarbonate resin, and polystyrene resin [1]. If the end products, that is, plastic products, food containers, medical supplies, etc., are directly discharged into rivers and seas or discharged with the waste effluent, BPA will be released into the environment, especially an aquatic environment [2]. In recent years, BPA has been frequently detected in water and drinking water all over the world [3]. For example, a research report in Germany gave the BPA concentration in surface water in 1997 as 0.5–410 ng/L [4]. From 2002 to 2003, BPA detected in drinking water sources in Hangzhou was 0.33–25.09 ng/L [5]. In 2002, an investigation of a typical sewage treatment plant in Beijing detected 30 kinds of endocrine disrupters. Among these, the BPA concentration was the highest at 0.825 mg/L [6]. China's *Drinking Water Health Standards* (GB 5749-2006) regulates the limiting value of BPA to be less than 0.01 mg/L. BPA is an important environmental endocrine disrupting chemical. It behaves as an estrogen in influencing physiological functions of organisms. Even a very small dose of BPA can lead to female precocious puberty, sperm decrease, prostatic hypertrophy and it has certain embryotoxicity and teratogenicity. By direct con-

* Corresponding author. Tel: +86-10-62759716; E-mail: shangjing@pku.edu.cn
This work was supported by the Fujitsu Laboratories Limited Foundation (k120400), the Beijing Natural Science Foundation (8132035), and the National Natural Science Foundation of China (21277004, 21190051, 41121004).
DOI: 10.1016/S1872-2067(12)60709-8 | http://www.sciencedirect.com/science/journal/18722067 | Chin. J. Catal., Vol. 35, No. 1, January 2014

tact or accumulation through the biological chain, BPA can enter the human body, which would lead to endocrine imbalance and disruption of the metabolic process. It also influences the immunity systems of infants and can cause male infertility and cancer [7]. Therefore, it is essential to remove BPA from the aqueous phase. Conventional BPA removal methods include biological, physical, and chemical methods. The chemical methods include Fenton oxidation [8], ultraviolet oxidation [9], H_2O_2 oxidation [10], oxychlorination [11], and photocatalytic oxidation treatment [12]. Simple Fenton, ultraviolet or H_2O_2 oxidation perform poorly in the removal of BPA, and the combination of several approaches are needed. For example, the incomplete oxidative degradation of BPA during oxychlorination process produces byproducts with stronger endocrine disruption effects [13]. Therefore, it is essential to find ways to more effectively remove these endocrine disrupters.

As an advanced oxidation technology, photocatalysis can remove organic and inorganic pollutants. It has advantages such as high catalytic efficiency, complete oxidation, and low energy consumption compared to the conventional technologies. In recent years, there have been many studies on the photocatalytic degradation of BPA by TiO_2 under ultraviolet irradiation, which verified that photocatalysis can completely oxidize BPA to CO_2 and H_2O with no secondary pollutants [14]. The estrogenic activity could be reduced to less than 10% of the original solution [14]. TiO_2, H_2O_2, and ultrasound can have synergistic effects [15]. The photocatalytic efficiency of 3D mesoporous TiO_2 was higher than that of commercial P25 TiO_2 [16]. Kuo et al [17] explored the effects of pH and polyethylene glycol on the photocatalytic degradation of BPA by TiO_2 under visible light. The photocatalytic degradation of BPA often needs an additive, such as H_2O_2 [18]. In order to improve catalytic efficiency, it is necessary to develop new and more efficient photocatalysts.

Ti-substituted hydroxyapatite (TiHAP) is a new photocatalyst. It is a crystal with Ti^{4+} replacing part of the Ca^{2+} in hydroxyapatite (HAP). HAP is a common medical material used in fixing tooth and bone tissues. The molecular formula of HAP is $Ca_{10}(PO_4)_6(OH)_2$. The Ca^{2+} ion can be replaced by other positive ions. Kandori et al [19] used metal ions such as Al^{3+}, La^{3+}, and Fe^{3+} to replace Ca^{2+} in HAP and investigated the adsorption capacity of the modified HAP for proteins. Wakamura et al. [20] synthesized TiHAP, which exhibited high photocatalytic activity under ultraviolet light. Tsukada et al. [21] evaluated the band gap and electronic structure of TiHAP both experimentally and theoretically. TiHAP has an adsorption capacity that is superior to TiO_2 [22].

This work used a TiHAP photocatalyst to degrade BPA and compared the photocatalytic activity of TiHAP to that of commercial P25 TiO_2. The adsorption capacity and photocatalytic ability with low concentration BPA were explored. Fulvic acid (FA) and Fe^{3+} ions commonly exist in water and can influence the adsorption, sedimentation, and light absorption of nanoparticles [23]. This paper also investigated the effects of FA and Fe^{3+} on the photocatalytic degradation of BPA over TiHAP films.

2. Experimental

2.1. Preparation of TiHAP powder

TiHAP with 10 mol% Ca substituted by Ti was provided by Environmental and Energy Research Center, Fujitus Laboratories Ltd., Japan. The TiHAP powder was synthesized using the coprecipitation method in the literature [19]. HAP was purchased from Shanghai Hualan Chemical Technology Co., Ltd. P25 TiO_2 was purchased from Degussa Co. with a particle size of 30 nm, specific surface area of 46.9 m^2/g, 80% anatase and average pore diameter of 15.5 nm.

2.2. Characterization of TiHAP

The morphology of TiHAP was characterized by transmission electron microscopy (TEM, Hitachi, JEM-200CX) with the stripe resolution ratio of 2.04, point resolution ratio of 0.24 nm, and acceleration voltage of 300 kV. The crystal structure of TiHAP was identified by X-ray diffraction (XRD) with a Rigaku Dmax/2000 diffractometer (Japan) using Cu K_α radiation (λ = 0.154 nm) in the scan range of 20°–80°. The BET surface areas of the samples were recorded with a Micromeritics ASAP 2020 instrument. The ultraviolet-visible (UV-Vis) diffuse reflection spectra of the samples were determined by UV-Vis spectrophotometry (Shimadzu, UV-3100) with wavelengths from 200 to 800 nm. The zeta potential of the particles suspended in deionized water (particle loading 100 mg/L) was analyzed with a Nano ZS90 apparatus (Malvern, UK). The pH values were adjusted using NaOH or HCl solutions.

2.3. Adsorption capacity of TiHAP and TiO_2 powder for BPA

BPA solutions with concentrations of 0.2, 0.4, 0.6, 0.8, 1.0, and 1.2 mg/L were prepared, and to each was added 100 mg/L TiHAP or TiO_2, which was mixed thoroughly. The solutions were placed in a water bath (25 °C) and stirred (150 r/min) in darkness for 24 h to achieve adsorption equilibrium. Then the filtrate was obtained with 0.22 μm syringe filters.

2.4. Photocatalytic activity of TiHAP and TiO_2 films for BPA degradation

2.4.1. Preparation of TiHAP and TiO_2 films

TiHAP powder (1.9425 g) and 10 mL of ultra-pure water were added onto a Petri dish (diameter of 9 cm) and mixed thoroughly. The solution was dried at 98 °C for 1 h, and a homogeneous thin film of TiHAP was formed at the bottom. This was cooled at room temperature for further use.

P25 TiO_2 powder (1.8075 g) and 10 mL of ultra-pure water were added to a Petri dish (diameter of 9 cm) and mixed thoroughly. The solution was dried at 80 °C for 5 h, and a homogeneous thin film of TiO_2 was formed at the bottom. This was cooled at room temperature for further use.

2.4.2. Photocatalytic degradation of BPA

A 50 mL of solution (1 mg/L BPA) was dropped onto the prepared TiHAP or TiO_2 film. After adsorption for 2 h in darkness, the film was put in a photoreactor with a UV lamp at the

wavelength of 365 nm. The lamp was 15 cm above the film and the light intensity was 1.2 mW/cm^2. For the experiments, the illumination time was set to 6 h. A 1.0 mL sample was taken for LC-MS analysis every 0.5 h. The films were very stable, and no dissolution or dispersion was observed during experiments.

The photocatalytic degradation of pollutants was fitted with a first order kinetics equation $\ln(C_0/C_t) = kt$, where C_t represented the concentration (mg/L) at time t, C_0 was the initial concentration (mg/L), and k was the reaction rate constant (h^{-1}).

In order to study the effects of FA and Fe^{3+} on the photocatalytic degradation of BPA, 50 mL of BPA solutions (1 mg/L) were prepared with different FA concentrations (2.5, 5, and 7.5 mg/L). BPA solutions (1 mg/L) with $FeCl_3$ (3.24, 8.11, and 16.22 mg/L) were also prepared.

2.4.3. Analytical methods

BPA concentration was determined by a liquid chromatography-mass spectrometer (LC-MS, HP1100 LC-MS^n Trap SL System, Agilent Technologies Co., USA) equipment with a Zorbax Eclipse XDB-C18 column (2.1 mm × 150 mm, particle size 5 μm, pore diameter 8.0 nm, monomeric, double-capped). Methanol/water (75%, v/v) was the mobile phase at a flow rate of 0.18 mL/min. The analysis time was 6.5 min. The LC-MS was equipped with ionization by electronic spray ions (ESI) and it was operated in the secondary MS anion scanning mode. The quantitative analysis of BPA was conducted in the MRM fragmentation mode with the target ion of m/z 227 ($[M-H]^-$) and the scanning range of 50–400. The maximum MS data accumulation time was 300 ms. The capillary voltage was 3500 V. The vaporization pressure was 2.4 × 10^5 Pa. The flow rate of the drying gas (N_2, 330 °C) was 8.0 L/min. The breakup voltage was 1.3 eV. The standard curve for concentration versus peak area was obtained by preparing a series of BPA (purity > 97%, Acros Organics, Geel Belgium) solutions with methanol (Scharlau, Belgium, HPLC grade). $FeCl_3$ and FA ($C_{14}H_{12}O_8$) used were analytically pure.

3. Results and discussion

3.1. Morphological and structural characteristics of the TiHAP particles

The TEM image of the TiHAP powder is shown in Fig. 1. TiHAP exhibited an aggregated structure made of spherical and rod-like particles of irregular sizes. The XRD pattern of TiHAP is shown in Fig. 2. The characteristic diffraction peak of TiHAP was in accordance with that of HAP (JCPDS 9-432), showing the hexagonal apatite structure [21]. However, no characteristic peak of TiO_2 in TiHAP was observed, indicating that Ti^{4+} was completely incorporated into the crytical lattice of HAP [22].

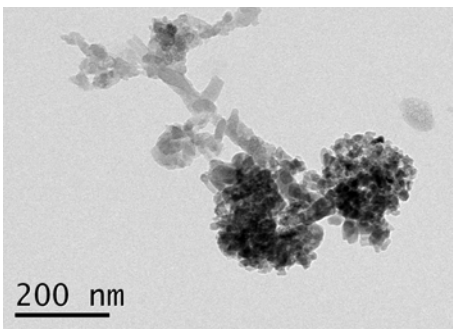

Fig. 1. TEM image of TiHAP powder.

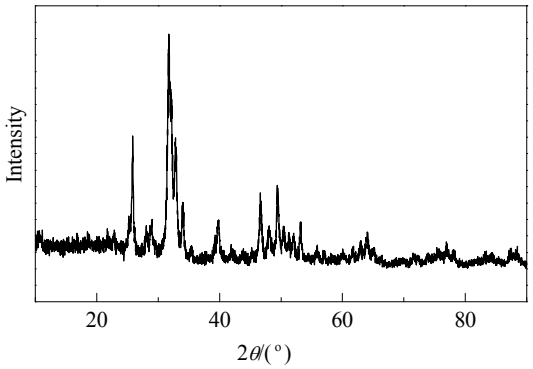

Fig. 2. XRD pattern of the TiHAP powder.

Figure 3 shows the UV-Vis diffuse reflectance spectra of HAP, TiHAP, and P25 TiO_2. The measured band gap energy of TiHAP and P25 TiO_2 were 3.45 and 3.02 eV, respectively, while the band gap energy of HAP was larger than 6.0 eV, which was consistent with the results of Tsukada et al. [21]. TiHAP showed a larger band gap and stronger absorption towards UV light than TiO_2, which indicated that TiHAP would exhibit photocatalytic activity in the near UV region. The result also implied that the surface of TiHAP was modified by the substitution with Ti^{4+} [22].

Figure 4 illustrates the surface zeta potential versus pH for the TiHAP and P25 TiO_2 powders. Generally, the system was stable when the absolute zeta potential was larger than 30 mV. As seen in Fig. 4, TiO_2 was stable in strong acidic or alkaline solutions, while TiHAP was stable only in strong acid solution. The pH of the isoelectric point (IEP) for TiO_2 was 6.4, which was close to the values of 5.8–7.0 reported previously [24,25]. The pH of the IEP for TiHAP was 2.7. There were hydroxyls on the surface of TiO_2 and TiHAP. According to proton transfer theory [26], at a pH below the IEP, the proton concentration is high, and protons have the trend of migrating to the surface of

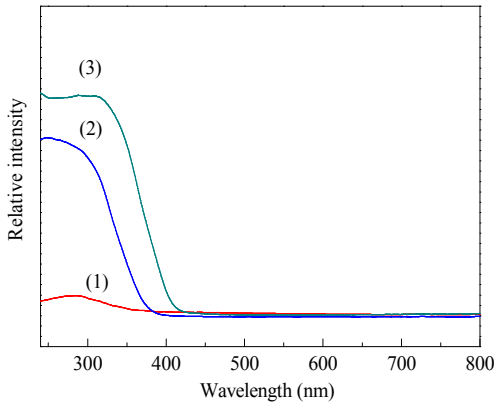

Fig. 3. UV-Vis diffuse reflectance spectra of the HAP (1), TiHAP (2), and P25 TiO_2 (3) powders.

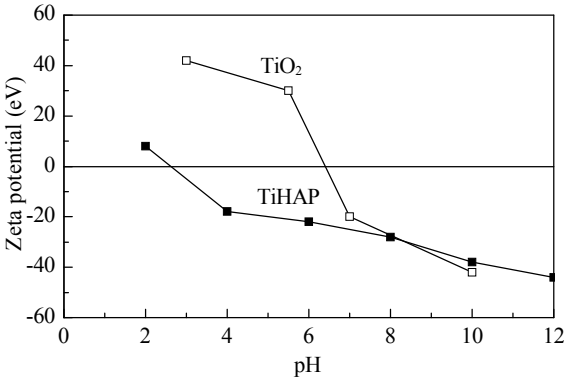

Fig. 4. Zeta potential of TiHAP and P25 TiO_2 versus pH.

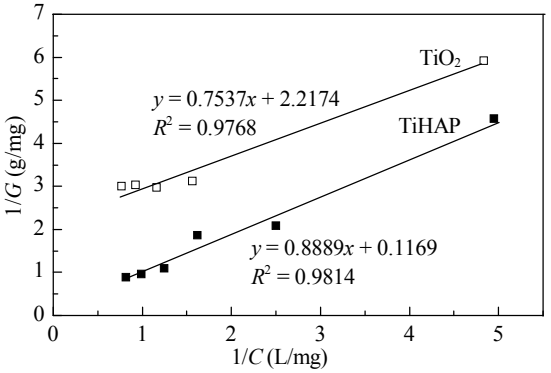

Fig. 5. Langmuir adsorption isotherm of BPA on the TiHAP and P25 TiO_2 particles.

particles. Thus, the surface hydroxyls have protons and became positive. At pH values above the IEP, surface hydroxyls lose protons and became negative. The IEP of TiHAP was lower than that of TiO_2, indicating that TiHAP would more easily lose protons and adsorb more acid groups such as hydroxyls [24]. The specific surface area of TiHAP was 45.9 m^2/g, and the average pore diameter was 14.2 nm from the BET results.

3.2. Adsorption behavior of BPA on the particles

Langmuir, Freundlich, and Temkin adsorption isotherms were used to fit the adsorption of BPA on the TiHAP and TiO_2 particles. The Langmuir equation was $1/G = 1/G^0 + (A/G^0)(1/C)$, where G is the adsorption amount, G^0 is the saturated adsorption per surface area, C is the equilibrium concentration, and A is a constant. $1/G$ and $1/C$ were used as the Y-axis and X-axis, respectively, and a linear fit was obtained, as shown in Fig. 5. The Freundlich equation was $\log G = A + (1/n)\log C$, where G is the adsorption amount, C is the equilibrium concentration, A and n are constants, and a linear fit was obtained similarly. The Temkin equation was $G = A + B\lg C$, where G is the adsorption amount, C is the equilibrium concentration, and A and B are two constants. Table 1 lists the fitting results of three adsorption equations of Langmuir, Freundlich, and Temkin. The fitting correlation coefficient of the Langmuir equation fit was larger than that of the Freundlich and Temkin equation fits, indicating that the adsorption of BPA on the TiHAP and TiO_2 particles were better fitted by the Langmuir isotherm. The adsorption heat does not change during Langmuir adsorption, and the energy of each adsorption point is the same, which represents homogeneous surface adsorption.

The intercept of the regression line was the reciprocal of the saturation adsorption capacity (G_0). It gave the saturated adsorption amounts of BPA on TiHAP and TiO_2 as 8.55 and 0.45 mg/g, respectively. The adsorption capacity of TiHAP for BPA was higher than that of TiO_2.

As shown in Fig. 4, the zeta potentials of TiHAP and TiO_2 did not show significant difference when the pH was about 7, suggesting that the surface charge was not the reason for the different adsorption capacities of the particles. In addition, the specific surface area and average pore diameter of TiHAP and TiO_2 were comparable, so these would not lead to the different adsorption capacities either. It is known that TiHAP is produced from a substitution of HAP by Ti, which resulted in multiple Ti-OH groups on the TiHAP surface [27]. Large amounts of phosphates and hydroxyls in the crystal lattice of TiHAP can adsorb the hydroxyls of BPA by hydrogen bonding. Although Ti-OH groups existed on the P25 TiO_2 surface as well, the experimental results showed that the adsorption capacity of TiHAP for BPA was larger than that of TiO_2.

3.3. Photocatalytic activity of the TiHAP and TiO_2 films for BPA degradation

3.3.1. Photocatalytic activity

The blank experiment exhibited that no direct photolysis of BPA was observed with 365 nm UV light illumination. In addition, the HAP sample showed no photocatalytic activity. The UV-Vis diffuse spectra (Fig. 3) indicated that HAP could only be excited by UV light with wavelengths shorter than 300 nm. Therefore, HAP would not show catalytic activity under these experimental conditions. Figure 6 shows the photocatalytic degradation curves of BPA with the TiHAP and TiO_2 films. The photodegradation rate of BPA was 0.115 h^{-1} over the TiHAP film, which was 2.4 times larger than that of the TiO_2 film (0.048 h^{-1}). The TiHAP film showed an enhanced photocatalytic activity over that of P25 TiO_2 for the degradation of BPA.

3.3.2. Effect of FA on photocatalytic degradation of BPA

Figure 7 exhibits the photocatalytic degradation rate of BPA coexisting with different FA concentrations over the TiHAP and

Table 1
Linear fit results for the three adsorption equations.

Sample	Langmuir equation $1/G = 1/G^0 + (A/G^0)(1/C)$	Freundlich equation $\lg G = A + (1/n)\lg C$	Temkin equation $G = A + B\lg C$
TiHAP	$1/G = 0.1169 + 0.8889(1/C)$, $R^2 = 0.9814$	$\lg G = -0.0036 + 0.9213\lg C$, $R^2 = 0.9676$	$G = 0.9794 + 1.1977\lg C$, $R^2 = 0.9233$
TiO_2	$1/G = 2.2174 + 0.7537(1/C)$, $R^2 = 0.9768$	$\lg G = -0.4675 + 0.3325\lg C$, $R^2 = 0.7022$	$G = 0.3377 + 0.1862\lg C$, $R^2 = 0.7196$

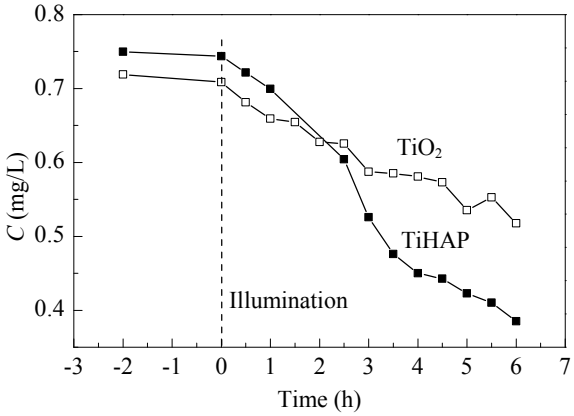

Fig. 6. Photocatalytic degradation curves of bisphenol A (BPA) over the TiHAP and TiO_2 films.

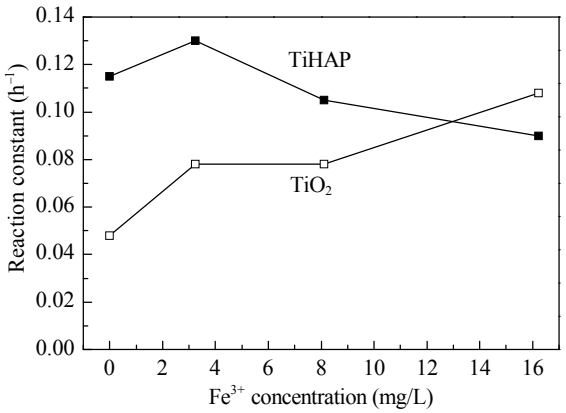

Fig. 8. Photocatalytic degradation rate of BPA versus Fe^{3+} concentration over the TiHAP and TiO_2 films.

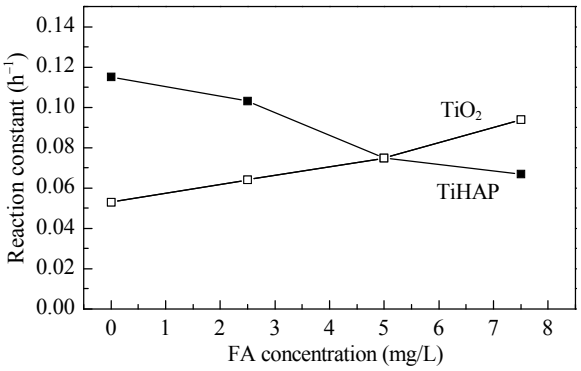

Fig. 7. Photocatalytic degradation rate of BPA versus fulvic acid (FA) concentration over the TiHAP and TiO_2 films.

TiO_2 films. With the increase of FA concentration, the degradation rate of BPA over the TiHAP films was successively reduced, which was in contrast to the trend of degradation rate of BPA over TiO_2 films. The reason was that the lowest unoccupied molecular orbital of FA was higher than the conduction band of TiO_2. After excitation, the photoinduced electrons of FA can transfer to the conduction band of TiO_2 and react with adsorbed O_2, followed by the formation of $\bullet O_2^-$ [28], which thereby improved the oxidation removal efficiency of BPA. However, TiHAP has a large band gap and a high conduction band [21]. The photoinduced electrons of FA cannot transfer to the conduction band of TiHAP. Conversely, the photoinduced electrons of TiHAP is transferred to the ground state of FA, that is, FA quenched the excited electrons in TiHAP, and the photocatalytic removal efficiency of BPA was reduced. Another possible reason for the promotion effect of FA in the photocatalytic degradation of BPA over TiO_2 film may be that FA can serve as the trapping agent of photoinduced holes. The increased separation efficiency of the photoinduced electron-hole pair resulted in enhanced photocatalytic efficiency with increased FA concentration.

3.3.3 Effect of Fe^{3+} on the photocatalytic degradation of BPA

Figure 8 shows the photocatalytic degradation rate of BPA over the TiHAP and TiO_2 films with different Fe^{3+} concentrations. With the increase of Fe^{3+} concentration, the photocatalytic activity of TiO_2 gradually increased. Fe^{3+} can capture photoinduced electrons [29] and increase the separation efficiency of the electron-hole pair, thereby facilitating the action of the photoinduced hole. Thus, more reactive oxygen species, such as hydroxyl free radicals, were produced, which enhanced the oxidative degradation of BPA. TiHAP showed a different trend of photocatalytic activity change. With the increase of Fe^{3+} concentration, the degradation rate of BPA first increased and then decreased. This may be attributed to the relatively low density of photoinduced electron-hole pairs on the TiHAP surface. Therefore, Fe^{3+} at low concentrations facilitated the separation of electron-hole pairs. Conversely, Fe^{3+} at high concentrations serves as recombination centers of electron-hole pairs, resulting in less reactive oxidizing species being generated. Another possible reason was that TiHAP had weak UV absorption at the wavelength of 365 nm. With higher Fe^{3+} concentrations, the deeper color of the solution would lead to decreased light absorption and decreased catalytic activity.

4. Conclusions

The adsorption of BPA on the TiHAP and TiO_2 powders was well described by the Langmuir adsorption equation. TiHAP exhibited a large adsorption capacity for BPA, which was 19 times as large as that of TiO_2 under the same conditions. This was due to hydrogen bonds formed between the hydroxyl groups of BPA and the hydroxyl groups on the TiHAP surface. The first order photocatalytic degradation rate constant of BPA over the TiHAP film was 2.4 times as large as that of TiO_2. An increase of radiation intensity would improve the catalytic activity. The photocatalytic mechanism of TiHAP needs to be further discussed. The results are useful for the application of TiHAP in the photocatalytic degradation of environmental endocrine disrupting chemicals.

References

[1] Nagel S C, vom Saal F S, Thayer K A, Dhar M G, Boechler M, Welshons W V. *Environ Health Persp*, 1997, 105: 70

Graphical Abstract

Chin. J. Catal., 2014, 35: 90–98 doi: 10.1016/S1872-2067(12)60709-8

Photocatalytic degradation of bisphenol A using Ti-substituted hydroxyapatite

Qian Li, Xiang Feng, Xiao Zhang, Han Song, Jianwei Zhang, Jing Shang*, Weiling Sun, Tong Zhu, Masato Wakamura, Mineharu Tsukada, Yingliang Lu
Peking University, China;
Fujitsu Laboratories Limited, Japan;
Fujitsu Research and Development Center, China

TiHAP film showed an enhanced photocatalytic activity than P25 TiO_2 film for degradation of bisphenol (BPA), an important kind of environmental endocrine disrupting chemicals.

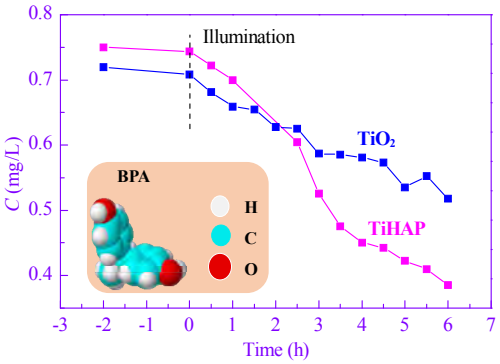

[2] Garoma T, Matsumoto S A, Wu Y, Klinger R. *Ozone-Sci Eng*, 2010, 32: 338
[3] Staples C A, Dome P B, Klecka G M, Oblock S T, Harris L R. *Chemosphere*, 1998, 36: 2149
[4] Fromme H, Küchler T, Otto T, Pilz K, Müller J, Wenzel A. *Water Res*, 2002, 36: 1429
[5] Zhang H F, Hu J Y, Chang H, Wang X L, Gao J F, Dong M Q. *Environ Chem* (张海峰, 胡建英, 常红,王秀丽, 高建峰, 董民强. 环境化学), 2004, 23: 584
[6] Du B, Zhang P Y, Zhang Z L, Yu G. *Chin J Environ Sci* (杜兵, 张彭义, 张祖麟, 余刚. 环境科学), 2004, 25: 114
[7] Kang J H, Kondo F, Katayama Y. *Toxicology*, 2006, 226: 79
[8] Katsumata H, Kawabe S, Kaneco S, Suzuki T, Ohta K. *J Photochem Photobiol A*, 2004, 162: 297
[9] Rosenfeldt E J, Linden K G. *Environ Sci Technol*, 2004, 38: 5476
[10] Chen P J, Linden K G, Hinton D E, Kashiwada S, Rosenfeldt E J, Kullman S W. *Chemosphere*, 2006, 65: 1094
[11] Korshin G V, Kim J, Gan L. *Water Res*, 2006, 40: 1070
[12] Yang J, Dai J, Li J T. *Appl Surf Sci*, 2011, 257: 8965
[13] Kuruto-Niwa R, Terao Y, Nozawa R. *Environ Toxicol Pharm*, 2002, 12: 27
[14] Ohko Y, Ando I, Niwa C, Tatsuma T, Yamamura T, Nakashima T, Kubota Y, Fujishima A. *Environ Sci Technol*, 2001, 35: 2365
[15] Torres R A, Nieto J I, Combet E, Pétrier C, Pulgarin C. *Appl Catal B*, 2008, 80: 168
[16] He Y, Duan H J, Wang G H, Guo C S, Wang Y Q. *Acta Sci Circumstantiae* (贺艳, 段海静, 王广华, 郭昌胜, 王玉秋. 环境科学学报), 2011, 31: 2179
[17] Kuo C Y, Wu C H, Lin H Y. *Desalination*, 2010, 256: 37
[18] Xie Y B, Li X Z. *J Hazard Mater*, 2006, 138: 526
[19] Kandori K, Toshima S, Wakamura M, Fukusumi M, Morisada Y. *J Phys Chem B*, 2010, 114: 2399
[20] Wakamura M, Hashimoto K, Watanabe T. *Langmuir*, 2003, 19: 3428
[21] Tsukada M, Wakamura M, Yoshida N, Watanabe T. *J Mol Catal A*, 2011, 338: 18
[22] Kandori K, Kuroda T, Wakamura M. *Colloids Surf B*, 2011, 87: 472
[23] Li S, Sun W L. *J Hazard Mater*, 2011, 197: 70
[24] Miyauchi M, Ikezawa A, Tobimatsu H, Irie H, Hashimoto K. *Phys Chem Chem Phys*, 2004, 6: 865
[25] Liao D L, Wu G S, Liao B Q. *Colloids Surf A*, 2009, 348: 270
[26] Chadwick M D, Goodwin J W, Lawson E J, Mills P D A, Vincent B. *Colloids Surf A*, 2002, 203: 229
[27] Wakamura M, Kandori K, Ishikawa T. *Colloids Surf A*, 2000, 164: 297
[28] Wang H J, Wu X J, Wang Y L, Jiao Z B, Yan S W, Huang L H. *Chin J Catal* (王后锦, 吴晓婧, 王亚玲, 焦自斌, 颜声威, 黄浪欢. 催化学报), 2011, 32: 637
[29] Shang J, Xue L, Li J, Zhao F W. *Chin J Catal* (尚静, 薛莲, 李佳, 赵凤伟. 催化学报), 2008, 29: 1037

载钛羟基磷灰石光催化降解内分泌干扰物双酚A

李 前[a], 冯 想[a], 张 晓[a], 宋 寒[a], 张建伟[a], 尚 静[a,*], 孙卫玲[a], 朱 彤[a]
若村正人[b], 塚田峰春[b], 陆应亮[c]
[a]北京大学环境科学与工程学院, 北京100871
[b]富士通研究所环境能源研究中心, 日本神奈川县厚木市
[c]富士通研究开发中心有限公司, 北京100025

摘要: 对载钛羟基磷灰石(TiHAP)进行了透射电镜、X射线衍射、紫外-可见光谱和Zeta电位表征, 并应用液相色谱-质谱技术对比了TiHAP和P25 TiO_2对环境内分泌干扰物双酚A(BPA)的吸附和光催化降解性能, 探讨了富里酸和Fe^{3+}对TiHAP薄膜光催化性能的影响. 结果表明, TiHAP和TiO_2粉体对BPA的吸附符合Langmuir吸附等温方程, 且前者吸附性能更大. TiHAP薄膜光催化降解BPA的性能优于TiO_2薄膜; 富里酸和Fe^{3+}对TiHAP和TiO_2薄膜光催化性能的影响趋势不同, 从能带结构、电子转移和吸光性等角度分析了性能不同的原因. 本结果可以为应用TiHAP降解环境内分泌干扰物提供依据.

关键词: 载钛羟基磷灰石; 光催化; 双酚A; 吸附; 二氧化钛

收稿日期: 2013-07-22. 接受日期: 2013-09-11. 出版日期: 2014-01-20.

*通讯联系人. 电话: (010)62759716; 电子信箱: shangjing@pku.edu.cn

基金来源: 日本富士通研究所环境能源研究中心基金(k120400); 北京市自然科学基金(8132035); 国家自然科学基金(21277004, 21190051, 41121004).

本文的英文电子版由Elsevier出版社在ScienceDirect上出版(http://www.sciencedirect.com/science/journal/18722067).

1. 前言

双酚A (BPA)广泛应用于环氧树脂、聚碳酸酯树脂和聚苯乙烯树脂的制造中[1]. 这些终产品(如塑料制品、食品容器、医疗用品等)如果处理不当可能会直接排入河流及海洋中, 或随垃圾处理产生的废液排出, 导致BPA释放到环境介质特别是水生环境中[2]. 近年来, 在国内外的原水及饮用水中BPA频频被检出[3]. 例如, 1997年在德国地表水中检测到BPA浓度为0.5–410 ng/L[4]; 2002–2003年在杭州饮用水源中检测到BPA浓度为0.33–25.09 ng/L[5]. 2002年对北京市某典型污水处理厂的调查中, 共检出30种内分泌干扰物, 其中BPA含量最高, 达0.825 mg/L[6]. 我国《生活饮用水卫生标准》(GB 5749-2006)中规定BPA的限值为0.01 mg/L. BPA是一种环境内分泌干扰物, 有模拟雌激素的作用, 影响机体的生理功能, 即使很低的剂量也能使动物产生雌性早熟、精子数下降和前列腺增长等, 还有一定的胚胎毒性和致畸性. 通过直接接触或生物链的积累效应. BPA还可能进入人体, 导致人体内分泌失衡, 扰乱人体代谢过程, 对婴儿发育、免疫力有影响, 还可能导致男性不育甚至致癌[7]. 因此, 去除液相中的BPA尤为重要. 传统的BPA处理方法主要有生物法、物理法以及化学法. 其中化学法是使用化学试剂或催化剂, 通过发生化学反应使BPA氧化降解, 主要包括Fenton氧化处理法[8]、紫外光氧化法[9]、H_2O_2氧化法[10]、氯氧化法[11]及光催化氧化法[12]等. 单一的Fenton氧化、紫外光氧化或H_2O_2氧化法对BPA的去除效果较差, 不能使其完全去除, 常需几种方法联用. 氯氧化处理方法不仅要加入大量化学试剂造成成本较高, 还会因为BPA氧化降解不彻底, 氯与BPA反应的副产物有更强的内分泌干扰作用[13], 反而加大其环境激素效应和毒性.

光催化作为一种高级氧化技术可用来处理有机和无机污染物, 与传统处理技术相比, 具有催化效率高、氧化彻底和能耗低等优势. 近年来, 关于TiO_2在紫外光照下光催化降解BPA已有很多报道. 已经证明, 采用TiO_2光催化技术可将BPA彻底氧化成CO_2和H_2O, 无二次污染产生[14]. 并且, 反应一定时间时体系中雌激素活性可减少到原溶液的10%以下[14]; TiO_2, H_2O_2和超声具有协同作用[15]; 3D介孔TiO_2光催化剂的效率高于市售P25 TiO_2粉体[16]. 对于在可见光下的研究, Kuo等[17]探讨了不同pH及聚乙二醇添加剂对TiO_2光催化降解BPA的影响. TiO_2光催化降解BPA的过程常需要引入添加剂, 如H_2O_2[18], 为进一步提高催化效率和降低成本, 需要开发新型高效的光催化剂.

载钛羟基磷灰石(TiHAP)是一种新型光催化剂, 是Ti^{4+}置换羟基磷灰石(HAP)中的一部分Ca^{2+}而形成的一种晶体. HAP是一种广泛采用的医用材料, 可用于牙齿或骨组织修复; 它的分子式为$Ca_{10}(PO_4)_6(OH)_2$, 其中的Ca^{2+}可被多种阳离子取代. Kandori等[19]用金属离子Al^{3+}, La^{3+}及Fe^{3+}替换HAP中的Ca^{2+}, 考察了改性后的HAP对蛋白质的吸附性能及影响因素. Wakamura等[20]将Ti^{4+}置换HAP中的部分Ca^{2+}, 所制TiHAP在近紫外光下表现出光催化活性. Tsukada等[21]分析和计算了Ti^{4+}掺杂后所引起的能带结构和吸光特性的变化. TiHAP作为一种新型光催化剂的同时, 还显示出比TiO_2更优异的吸附性能[22].

本文首次应用TiHAP光催化降解BPA, 并与常用的商业P25 TiO_2作对比, 研究其对低浓度BPA的吸附和光催化降解特性. 富里酸(FA)和Fe^{3+}是水体中普遍存在的物质, 对纳米颗粒物的吸附、沉降及吸光性有影响[23], 因此还考察了FA和Fe^{3+}对TiHAP薄膜光催化降解BPA性能的影响.

2. 实验部分

2.1. TiHAP粉体的制备

TiHAP粉体由日本富士通研究所环境能源研究中心提供, 采用共沉淀法制备[19], 特征是HAP中10 mol%的Ca^{2+}被Ti^{4+}所取代; HAP粉体购自上海华蓝化学科技有限公司; P25 TiO_2粉体购自Degussa公司, P25 TiO_2的粒径为30 nm, 比表面积46.9 m^2/g, 平均孔径15.5 nm, 是锐钛矿与金红石的混晶, 其中锐钛矿含量为80%.

2.2. TiHAP粉体的表征

采用日本日立公司JEM-200CX型透射电子显微镜(TEM)表征TiHAP粉体的形貌, 条纹分辨率2.04, 点分辨率0.24 nm, 加速电压300 kV; 采用日本Rigaku公司Dmax/2000型X射线衍射(XRD)仪测定TiHAP的晶型结构, 扫描速度为4°/min, Cu K_α靶, λ = 0.154 nm, 扫描范围为2θ = 20°–80°; 采用Micromeritics公司ASAP 2020型BET比表面积测定仪测定颗粒物的比表面积; 采用岛津公司UV-3100型紫外可见光度计测定样品的紫外可见漫反射光谱(UV-Vis), 波长范围200–800 nm. 采用Nano ZS90 (Malvern, 英国)分析颗粒物的zeta电位, 用NaOH或HCl水溶液调节体系的pH值, TiHAP或TiO_2溶液的浓度为100 mg/L.

2.3. TiHAP粉体和TiO_2粉体对BPA的吸附性能

制备0.2, 0.4, 0.6, 0.8, 1.0和1.2 mg/L的BPA系列溶液, 分别加入100 mg/L的TiHAP粉体和TiO_2粉体并摇晃均匀. 置于25 °C的恒温水浴锅中, 以150 r/min速度搅拌, 在黑暗中吸附24 h后, 利用0.22 μm的一次性过滤头进行过滤取样.

2.4. TiHAP和TiO_2薄膜对BPA的光催化降解

2.4.1. TiHAP和TiO_2薄膜的制备

用直径为9 cm的培养皿称取约1.9425 g的TiHAP粉末, 用约10 mL超纯水溶解, 摇晃均匀后于98 °C干燥1 h后取出, 在培养皿底部附着有一层均匀的TiHAP薄膜, 自然冷却后待用.

用直径为9 cm的培养皿称取约1.8075 g的P25 TiO_2粉末, 用约10 mL超纯水溶解, 摇晃均匀后于80 °C干燥5 h后取出, 在培养皿底部附着有一层均匀的TiO_2薄膜, 自然冷却后待用.

2.4.2. 光催化降解实验

在已制备好待用的TiHAP和TiO_2薄膜上滴加50 mL的BPA溶液(1 mg/L). 将两个培养皿暗态下吸附2 h后, 放入光反应器中. 光源为主波长为365 nm的紫外灯, 光源距薄膜15 cm, 薄膜处光强为1.2 mW/cm^2, 每光照0.5 h取1.0 mL样进行液相色谱-质谱(LC-MS)分析, 光照时间为6 h. 两种薄膜在反应溶液中的稳定性很好, 在滴加溶液和光照的过程中没有发生溶解和分散.

对于浓度较低的反应液, 光催化降解有机物的过程符合一级动力学方程$\ln(C_0/C_t) = kt$, 式中, C_t和C_0分布代表初始和反应t时刻的物质浓度(mg/L), k代表一级动力学方程的速率常数(h^{-1}), 用以表征样品的催化性能.

分别配制FA浓度为2.5, 5和7.5 mg/L的50 mL BPA溶液(1 mg/L); 配制$FeCl_3$浓度为3.24, 8.11和16.22 mg/L的50 mL BPA溶液(1 mg/L)用以考察FA和Fe^{3+}的影响.

2.4.3. 样品浓度测定

使用液相色谱质谱联用仪(LC-MS, HP1100 LC-MS^n Trap SL System, 美国安捷伦公司)测定样品浓度并进行数据分析. 色谱条件: 采用Agilent公司Zorbax Eclipse XDB-C18色谱柱(2.1 mm × 150 mm, 粒径5 μm, 孔径8.0 nm, 单聚体, 双封端), 柱温没有限定, 进样量5 μL. 以甲醇和水作为流动相, 其中甲醇为75%(v/v), 流速0.18 mL/min, 停止时间6.5 min. 质谱条件: ESI的电喷雾源, 二级质谱负离子扫描模式, 离子阱SL系统. 对BPA的定量分析, 采用MRM的fragmentation模式, 目标离子m/z 227 ([M-H]$^-$), 扫描范围m/z = 50–400, 最长累积时间300 ms, 毛细管电压3500 V, 气化压力2.4×10^5 Pa, 干燥气(N_2)流速8.0 L/min, 干燥气温度330 °C, 破碎电压1.3 eV. 用色谱纯的甲醇(Scharlau, 比利时)配制一系列不同浓度的BPA (纯度>97%, Acros Organics, Geel Belgium), 绘制浓度-峰面积标准工作曲线. $FeCl_3$、富里酸($C_{14}H_{12}O_8$)均为分析纯.

3. 结果与讨论

3.1. TiHAP粉体的形貌和结构特性

图1为TiHAP粉体的TEM照片. 可以看出, TiHAP颗粒较易团聚, 粒子呈球状和棒状, 尺寸不规则. 图2为TiHAP样品的XRD谱, 可见其特征衍射峰与HAP (JCPDS 9-432)的一致, 为六边的磷灰石结构[21], 且未出现TiO_2的特征峰, 说明Ti^{4+}离子完全进入到HAP的晶格中[22].

图3为HAP, TiHAP和P25 TiO_2三种颗粒物的UV-Vis漫反射谱. 可以看出, TiHAP和P25 TiO_2对应的带隙分别为3.45和3.02 eV左右, 而HAP的带隙大于6.0 eV, 与Tsukada等[21]的结果一致. TiHAP显示出了比TiO_2更大的带隙能, 在紫外光区域有较强的吸收, 进一步说明Ti^{4+}离子进入了HAP的晶格中.

图4为TiHAP和P25 TiO_2的Zeta电位随pH的变化. 通常Zeta电位的绝对值在30 mV以上, 体系是稳定的. 由图4可知, TiO_2在较强酸性和碱性下比较稳定, 而TiHAP只有在强碱性下才稳定. TiO_2的等电位点在pH 6.4左右, 与文献报道的5.8–7.0接近[24,25]; TiHAP的等电位点在pH 2.7左右. TiO_2和TiHAP表面存在羟基, 由质子转移理论[26]可知, 在等电点以下的低pH条件下, 质子浓度高, 有向粒子表面迁移的趋势, 使表面的羟基得到质子带正电; 在等电位以上的高pH条件下, 羟基失去质子而带负

电. TiHAP等电位点比TiO_2更低表明其更易失去质子, 吸附有更多的羟基等酸性位点[24]. BET测试结果表明, TiHAP的比表面积为45.9 m^2/g, 平均孔径为14.2 nm.

3.2. TiHAP和TiO_2粉体对BPA的吸附

本文采用Langmuir, Freundlich和Temkin吸附等温式拟合TiHAP和TiO_2对BPA的吸附. Langmuir方程为$1/G = 1/G^0 + (A/G^0)(1/C)$, 其中$G$为吸附量, G^0为单位表面上达到饱和时间的最大吸附量, C为平衡浓度, A为常数; 以$1/G$对$1/C$作图可得到一条直线, 如图5所示. Freundlich方程为$\lg G = A + (1/n)\lg C$, 其中G为吸附量, C为平衡浓度, A, n为常数; 以$\lg G$对$\lg C$作图可得到一条直线. Temkin方程为$G = A + B\lg C$, 其中G为吸附量, C为平衡浓度, A和B为两个常数; 以G对$\lg C$作图为一条直线. 表1列出了Langmuir, Freundlich和Temkin三种吸附方程拟合的结果. 可以看出, Langmuir吸附模型的线性相关系数大于Freundlich和Temkin吸附模型的, 说明TiHAP和TiO_2粉体对BPA的吸附更符合Langmuir吸附方程, 吸附热不随吸附而变化, 每一个吸附点的能量不变, 是均匀的表面吸附.

图5中回归直线的截距是饱和吸附量G^0的倒数, 由此算得TiHAP和TiO_2粉体单位表面上达到饱和的最大吸附量分别为8.55和0.45 mg/g, TiHAP粉体对BPA的吸附能力优于TiO_2粉体.

由图4可知, 在pH为7左右时, TiHAP和TiO_2的Zeta电位值相差不多, 说明表面电荷不是颗粒物吸附性能差异的原因; 另外, 两者的比表面积和平均孔径相似, 本体的表面吸附应该也不是主要原因. TiHAP是HAP的金属取代物, HAP表面的P-OH基团可部分形成Ti-OH基团[27], 使TiHAP晶体中含大量磷酸根和羟基, 可以通过氢键吸附BPA上的羟基, 从而将BPA吸附到TiHAP表面. 虽然P25 TiO_2表面也有Ti-OH基团, 但由实验结果可知, TiHAP粉体对BPA的吸附能力大于TiO_2粉体.

3.3. TiHAP和TiO_2薄膜光催化降解BPA

3.3.1. 光催化降解活性

空白实验表明, BPA在$\lambda = 365$ nm的紫外光照下不发生光解; HAP样品在本实验光源下也无催化活性. 由图3可知, HAP在$\lambda < 300$ nm的紫外光照下才能被激发, 所以在本文条件下不具有催化活性. 图6为TiHAP和TiO_2薄膜对BPA溶液的光催化降解曲线. TiHAP薄膜和TiO_2薄膜对BPA的光催化降解速率常数分别为0.115 h^{-1}和0.048 h^{-1}, 由此算得, 前者是后者的2.4倍.

3.3.2. FA的影响

图7为不同FA浓度的溶液中TiHAP和TiO_2薄膜光催化降解BPA的速率常数. 由图可见, 随着FA浓度的增加, TiHAP薄膜光催化降解BPA的速率常数减小, 而TiO_2薄膜的却增加. 推测可能的原因为: FA的LUMO轨道高于TiO_2的导带, FA受光激发后光生电子能够转移到TiO_2的导带上, 光生电子可以进一步与O_2作用形成$\bullet O_2^-$[28], 进而提高了BPA的氧化去除效率. TiHAP的带隙很大, 导带位置很高[21], FA的光生电子不能转移到TiHAP的导带上; 相反, TiHAP的光生激子可以转移到FA的基态上, 即FA起到了猝灭TiHAP中激子的作用, 从而降低了其光催化去除BPA效率. 另一方面, FA可作为光生空穴的捕获剂, 使光生电子空穴的分离效率增加, 且随FA浓度的增加分离效率增大.

3.3.3. Fe^{3+}的影响

图8为在不同Fe^{3+}浓度下TiHAP和TiO_2薄膜光催化降解BPA的反应速率. 可以看出, 随Fe^{3+}浓度的增大, TiO_2光催化降解BPA的活性逐渐增大. Fe^{3+}可捕获光生电子[29], 增加了电子空穴的分离效率, 从而使光生空穴得到更好地利用, 产生更多的活性氧物种如羟基自由基, 进而促进了BPA的氧化降解. 而对于TiHAP, 在低浓度Fe^{3+}存在时, 其催化降解BPA的性能增加; 之后随Fe^{3+}浓度的增加而降低. 推测可能的原因为: TiHAP表面的光生电子-空穴对密度较低, 所以低浓度的Fe^{3+}可有助于电子空穴的分离; 高浓度的Fe^{3+}反而可作为电子空穴的复合中心, 从而不利于氧化性物质的生成. 另外一个可能的原因是, TiHAP对$\lambda = 365$ nm的紫外光吸收较弱, 在Fe^{3+}浓度高时, 溶液颜色加深, 不利于TiHAP对光的吸收, 导致其催化活性降低.

4. 结论

TiHAP和TiO_2粉体对BPA的吸附符合Langmuir吸附等温方程, 同等条件下, TiHAP对BPA的最大吸附量是TiO_2的19倍, 这是由于BPA分子的羟基与TiHAP表面的羟基形成氢键所致. TiHAP薄膜光催化降解BPA的一级反应速率常数是TiO_2的2.4倍. TiHAP的光催化反应机制还有待于进一步探讨, 提高辐照强度预计会提高其催化性能. 本结果可为TiHAP降解环境内分泌干扰物提供依据, 具有一定的理论和应用价值.